Investigation of the $dd \to {}^3\mathrm{He}n\pi^0$ reaction with WASA-at-COSY

P. Adlarson,[1] W. Augustyniak,[2] W. Bardan,[3] M. Bashkanov,[4,5] F.S. Bergmann,[6] M. Berłowski,[7] H. Bhatt,[8] M. Büscher,[9,10] H. Calén,[1] I. Ciepał,[3] H. Clement,[4,5] D. Coderre,[9,10,11] E. Czerwiński,[3] K. Demmich,[6] E. Doroshkevich,[4,5] R. Engels,[9,10] W. Erven,[12,10] W. Eyrich,[13] P. Fedorets,[9,10,14] K. Föhl,[15] K. Fransson,[1] F. Goldenbaum,[9,10] P. Goslawski,[6] A. Goswami,[16] K. Grigoryev,[9,10,17] C.–O. Gullström,[1] C. Hanhart,[9,10,18] F. Hauenstein,[13] L. Heijkenskjöld,[1] V. Hejny,[9,10,*] F. Hinterberger,[19] M. Hodana,[3,9,10] B. Höistad,[1] A. Jany,[3] B.R. Jany,[3] L. Jarczyk,[3] T. Johansson,[1] B. Kamys,[3] G. Kemmerling,[12,10] F.A. Khan,[9,10] A. Khoukaz,[6] D.A. Kirillov,[20] S. Kistryn,[3] J. Klaja,[3] H. Kleines,[12,10] B. Kłos,[21] M. Krapp,[13] W. Krzemień,[3] P. Kulessa,[22] A. Kupść,[1,7] K. Lalwani,[8,†] D. Lersch,[9,10] L. Li,[13] B. Lorentz,[9,10] A. Magiera,[3] R. Maier,[9,10] P. Marciniewski,[1] B. Mariański,[2] M. Mikirtychiants,[9,10,11,17] H.–P. Morsch,[2] P. Moskal,[3] B.K. Nandi,[8] H. Ohm,[9,10] I. Ozerianska,[3] E. Perez del Rio,[4,5] N.M. Piskunov,[20] P. Pluciński,[1,‡] P. Podkopał,[3,9,10] D. Prasuhn,[9,10] A. Pricking,[4,5] D. Pszczel,[1,7] K. Pysz,[22] A. Pyszniak,[1,3] C.F. Redmer,[1,§] J. Ritman,[9,10,11] A. Roy,[16] Z. Rudy,[3] S. Sawant,[8] A. Schmidt,[13] S. Schadmand,[9,10] T. Sefzick,[9,10] V. Serdyuk,[9,10,23] N. Shah,[8,¶] M. Siemaszko,[21] R. Siudak,[22] T. Skorodko,[4,5] M. Skurzok,[3] J. Smyrski,[3] V. Sopov,[14] R. Stassen,[9,10] J. Stepaniak,[7] E. Stephan,[21] G. Sterzenbach,[9,10] H. Stockhorst,[9,10] H. Ströher,[9,10] A. Szczurek,[22] T. Tolba,[9,10,**] A. Trzciński,[2] R. Varma,[8] G.J. Wagner,[4,5] W. Węglorz,[21] M. Wolke,[1] A. Wrońska,[3] P. Wüstner,[12,10] P. Wurm,[9,10] A. Yamamoto,[24] X. Yuan,[25] J. Zabierowski,[26] C. Zheng,[25] M.J. Zieliński,[3] W. Zipper,[21] J. Złomańczuk,[1] P. Żuprański,[2] and M. Żurek[3]

(WASA-at-COSY Collaboration)

[1] *Division of Nuclear Physics, Department of Physics and Astronomy, Uppsala University, Box 516, 75120 Uppsala, Sweden*
[2] *Department of Nuclear Physics, National Centre for Nuclear Research, ul. Hoza 69, 00-681, Warsaw, Poland*
[3] *Institute of Physics, Jagiellonian University, ul. Reymonta 4, 30-059 Kraków, Poland*
[4] *Physikalisches Institut, Eberhard–Karls–Universität Tübingen, Auf der Morgenstelle 14, 72076 Tübingen, Germany*
[5] *Kepler Center for Astro and Particle Physics, Eberhard Karls University Tübingen, Auf der Morgenstelle 14, 72076 Tübingen, Germany*
[6] *Institut für Kernphysik, Westfälische Wilhelms–Universität Münster, Wilhelm–Klemm–Str. 9, 48149 Münster, Germany*
[7] *High Energy Physics Department, National Centre for Nuclear Research, ul. Hoza 69, 00-681, Warsaw, Poland*
[8] *Department of Physics, Indian Institute of Technology Bombay, Powai, Mumbai–400076, Maharashtra, India*
[9] *Institut für Kernphysik, Forschungszentrum Jülich, 52425 Jülich, Germany*
[10] *Jülich Center for Hadron Physics, Forschungszentrum Jülich, 52425 Jülich, Germany*
[11] *Institut für Experimentalphysik I, Ruhr–Universität Bochum, Universitätsstr. 150, 44780 Bochum, Germany*
[12] *Zentralinstitut für Engineering, Elektronik und Analytik, Forschungszentrum Jülich, 52425 Jülich, Germany*
[13] *Physikalisches Institut, Friedrich–Alexander–Universität Erlangen–Nürnberg, Erwin–Rommel-Str. 1, 91058 Erlangen, Germany*
[14] *Institute for Theoretical and Experimental Physics, State Scientific Center of the Russian Federation, Bolshaya Cheremushkinskaya 25, 117218 Moscow, Russia*
[15] *II. Physikalisches Institut, Justus–Liebig–Universität Gießen, Heinrich–Buff–Ring 16, 35392 Giessen, Germany*
[16] *Department of Physics, Indian Institute of Technology Indore, Khandwa Road, Indore–452017, Madhya Pradesh, India*
[17] *High Energy Physics Division, Petersburg Nuclear Physics Institute, Orlova Rosha 2, Gatchina, Leningrad district 188300, Russia*
[18] *Institute for Advanced Simulation, Forschungszentrum Jülich, 52425 Jülich, Germany*
[19] *Helmholtz–Institut für Strahlen– und Kernphysik, Rheinische Friedrich–Wilhelms–Universität Bonn, Nußallee 14–16, 53115 Bonn, Germany*
[20] *Veksler and Baldin Laboratory of High Energiy Physics, Joint Institute for Nuclear Physics, Joliot–Curie 6, 141980 Dubna, Moscow region, Russia*
[21] *August Chełkowski Institute of Physics, University of Silesia, Uniwersytecka 4, 40-007, Katowice, Poland*
[22] *The Henryk Niewodniczański Institute of Nuclear Physics, Polish Academy of Sciences, 152 Radzikowskiego St, 31-342 Kraków, Poland*
[23] *Dzhelepov Laboratory of Nuclear Problems, Joint Institute for Nuclear Physics, Joliot–Curie 6, 141980 Dubna, Moscow region, Russia*
[24] *High Energy Accelerator Research Organisation KEK, Tsukuba, Ibaraki 305–0801, Japan*
[25] *Institute of Modern Physics, Chinese Academy of Sciences, 509 Nanchang Rd., Lanzhou 730000, China*
[26] *Department of Cosmic Ray Physics, National Centre for Nuclear Research, ul. Uniwersytecka 5, 90–950 Łódź, Poland*

(Dated: April 15, 2013)

An exclusive measurement of the $dd \to {}^3\mathrm{He}n\pi^0$ reaction was carried at a beam momentum of $p_d = 1.2$ GeV/c using the WASA-at-COSY facility. For the first time data on the total cross section as well as differential distributions were obtained. The data are described with a phenomenological

approach based on a combination of a quasi-free model and a partial wave expansion for three-body reaction. The total cross section is found to be $\sigma_{tot} = (2.89 \pm 0.01_{stat.} \pm 0.06_{sys.} \pm 0.29_{norm})\ \mu b$. The contribution of the quasi-free processes (with the neutron being target or beam spectator) accounts for 38% of the total cross section and dominates the differential distributions in specific regions of the phase space. The remaining part of the cross section can be described within a partial wave decomposition indicating the significance of p-wave contributions in the final state.

PACS numbers: 13.75.-n,21.45.-v,25.10.+s,25.45.-z
Keywords: deuteron-deuteron interaction, pion production, few nucleon system

INTRODUCTION

At the fundamental level of the Standard Model, isospin violation is due to quark mass differences as well as electromagnetic effects [1–3]. Therefore, the observation of isospin violation in principle allows one to study quark mass effects in hadronic processes. However, in general isospin violating observables are largely dominated by the pion mass differences, which are enhanced due to the small pion mass. An exception are charge symmetry breaking (CSB) observables (charge symmetry is the invariance of a system under rotation by 180° around the second axis in isospin space that interchanges up and down quarks), since charge symmetry transforms a π^+ into a π^- and therefore the pion mass difference does not contribute. Ref. [4] calls the investigation of CSB effects one of the most challenging subjects in hadron physics. On the basis of theoretical approaches with a direct connection to QCD, like lattice QCD and effective field theory, it is therefore possible to study quark mass effects on the hadronic level, since the effects of virtual photons are under control — for a detailed discussion on this subject see Ref. [5].

The first observation of the $dd \to {}^4\mathrm{He}\pi^0$ reaction was reported for beam energies very close to the reaction threshold [6]. At the same time information on CSB in $np \to d\pi^0$ manifesting as a forward-backward asymmetry became available [7]. These data triggered advanced theoretical calculations within effective field theory, providing the opportunity to investigate the influence of the quark masses in nuclear physics [8, 9]. This is done using Chiral Perturbation Theory (ChPT) which has been extended to pion production reactions [10]. First steps towards a theoretical understanding of the $dd \to {}^4\mathrm{He}\pi^0$ reaction have been taken [11, 12]. Soft photon exchange in the initial state could significantly enhance the cross sections for $dd \to {}^4\mathrm{He}\pi^0$ [13], however, it was demonstrated in Ref. [14] that a simultaneous analysis of CSB in the two-nucleon sector and in $dd \to {}^4\mathrm{He}\pi^0$ strongly constraints the calculations of the latter.

The main problem in the calculation of $dd \to {}^4\mathrm{He}\pi^0$ is to get theoretical control over the isospin symmetric part of the initial state interactions, for here high accuracy wave functions are needed for $dd \to 4N$ in low partial waves at relatively high energies. To get access to these a measurement is necessary for other, isospin conserving, dd induced pion production reaction channels at a similar excess energy, such that the final state is constrained to small angular momenta. Then the incoming system shares at least some of the partial waves in the initial state with the reaction $dd \to {}^4\mathrm{He}\pi^0$, while the transition operator is calculable with sufficient accuracy using ChPT. Such a reaction is $dd \to {}^3\mathrm{He}n\pi^0$ and a corresponding measurement is presented here.

EXPERIMENT

The experiment was carried out at the Institute for Nuclear Physics of Forschungszentrum Jülich in Germany using the Cooler Synchrotron COSY [15] together with the WASA detection system. For the measurement of $dd \to {}^3\mathrm{He}n\pi^0$ at an excess energy of $Q \approx 40$ MeV a deuteron beam with a momentum of 1.2 GeV/c was scattered on frozen deuteron pellets provided by an internal pellet target. The reaction products ^{3}He and π^0 were detected by the Forward Detector and the Central Detector of the WASA facility respectively, while the neutron remained undetected. The Forward Detector consists of several layers of plastic scintillators for particle identification and energy reconstruction and an array of straw tubes for precise tracking. The polar angular range between 3° and 18° fully covers the angular range of the outgoing ^{3}He with the exception of very small angles. At this beam momentum the ^{3}He ejectiles have kinetic energies in the range of 65 - 214 MeV and, thus, are already stopped in the first detector layers: in addition to the straw tube tracker only the two 3 mm thick layers of the Forward Window Counter and the first 5 mm thick layer of the Forward Trigger Hodoscope were used. The two photons from the π^0 decay were detected by the Scintillator Electromagnetic Calorimeter as part of the Central Detector. The photons were distinguished from charged particles using the Plastic Scintillator Barrel located inside the calorimeter. The experiment trigger was based on a coincidence between a high energy deposit in both layers of the Forward Window Counter together with a veto condition on the first layer of the Forward Range Hodoscope to select helium ejectiles and a low energy neutral cluster ($E > 20$ MeV) in the calorimeter to tag the decay of the pion. Further information on the WASA-at-COSY facility can be found in Ref.[16].

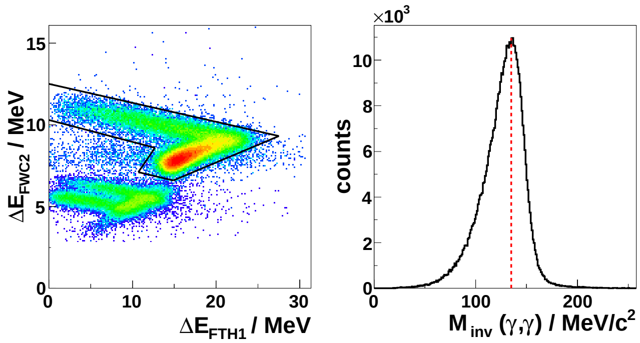

FIG. 1. Left: Energy loss in the Forward Window Counter versus energy loss in the first layer of the Forward Trigger Hodoscope. The obtained energy pattern shows clear separation between different particles types. The graphical cut indicated in black represents the region used to select ^{3}He candidates. Right: The two photon invariant mass distribution corresponding to the $\pi^0 \to \gamma\gamma$ decay. The red dashed line indicates the π^0 mass.

DATA ANALYSIS

Apart from the charge symmetry breaking reaction $dd \to {}^4\text{He}\pi^0$ with a four orders of magnitude smaller cross section, $dd \to {}^3\text{He}n\pi^0$ is the only process with a charge 2 particle and a neutral pion in final state. Thus, the identification of a forward going helium and two neutral tracks forming a pion already provides a clean signature for this reaction. Helium isotopes are identified by means of $\Delta E - \Delta E$ plots using the energy deposit in the Forward Window Counter and the first layer of the Foward Trigger Hodoscope (Fig. 1, left). The condition that the ^{3}He has to pass at least the first two scintillator layers introduces an additional acceptance cut of $E_{kin} >$ 125 MeV. This rejects most of the ^{3}He going backward in the c.m. system. However, having two identical particles in the initial state and, thus, a symmetric angular distribution with respect to $\theta_{CM} = 90°$ the full angular range can be recovered by a symmetrization of the detected events. The energy deposits are also used to reconstruct the ^{3}He kinetic energy by matching the energy loss pattern to Monte-Carlo simulations. The ^{3}He four-momentum is completed by the direction information from the straw tube tracker. In addition to the ^{3}He two neutral clusters in the central detector corresponding to the two photons from the π^0 decay were requested. As event pile-up and low energy satellites of genuine photon clusters can cause larger photon multiplicities the most probable true two-photon combination was identified by selecting the pair with the $^3\text{He} - \pi^0$ missing mass being closest to the neutron mass. As result a nearly background free pion peak was obtained (Fig. 1, right). In a final step the data were refined by applying a kinematic fit using the hypothesis $dd \to {}^3\text{He}n\pi^0$. Still remaining background and badly reconstructed events were rejected by a cut on the cumulated probability distribution at 10%. At the end of the analysis chain about 3.4×10^6 fully reconstructed and background free $dd \to {}^3\text{He}n\pi^0$ events are available. It should be noted that the Dalitz plot is fully covered except for a small region for large $\pi^0 - n$ invariant masses due to the acceptance hole for $\theta_{^3\text{He}} < 3°$. Although based on this data set any possible differential distribution can be generated — e.g. for a selective comparison with future microscopic theoretical calculations — a suitable set of observables for further analysis and presentation had to be selected. For any unpolarised measurement with three particles in final state four independent variables fully describe the reaction kinematics. For the present analysis the choice for these independent variables is based on the Jacobi momenta $\vec{q}$ and $\vec{p}$ with $\vec{q}$ being the π^0 momentum in the overall c.m. system and $\vec{p}$ the momentum in the rest frame of the $^3\text{He} - n$ subsystem. The following variables were constructed accordingly: $cos\theta_q$, $cos\theta_p$ (the polar angles of $\vec{q}$ and $\vec{p}$, respectively), $M_{^3\text{He}n}$ and φ (the angle between the projections of $\vec{q}$ and $\vec{p}$ onto the xy-plane). As discussed earlier all plots show data after a symmetrization in the global c.m. system.

The absolute normalisation was done relative to the $dd \to {}^3\text{He}n$ reaction. Corresponding data were taken in parallel during the first part of the run using a separate trigger. Due to the correlation between kinetic energy and scattering angle for the binary reaction, quasi mono-energetic particles form a distinct and clean peak in the $\Delta E - \Delta E$ plots. For the selected events the ^{3}He missing mass distribution reveals a background free peak at the mass of the neutron (Fig. 2, left). In order to determine the integrated luminosity the data presented in Ref. [17] were used. The authors measured the reaction $dd \to {}^3\text{H}p$ for beam momenta between 1.09 GeV/c - 1.78 GeV/c and

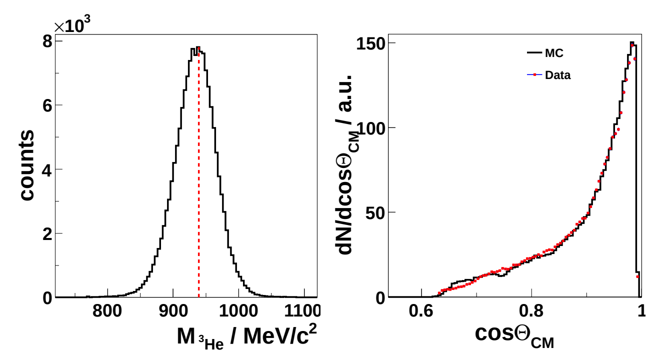

FIG. 2. Measurement of the $dd \to {}^3\text{He}n$ reaction. Left: ^{3}He missing mass distribution, the vertical red dashed line indicates the neutron mass. Right: Measured angular distribution in comparison with a Monte Carlo (MC) simulation. The MC sample was generated based on a parametrized cross section. The cross section is given in arbitrary units (a.u.).

$dd \to {}^3\mathrm{He}n$ for beam momenta in the range of 1.65 GeV/c - 2.5 GeV/c. Moreover, they showed that the differential cross sections for both channels at 1.65 GeV/c are identical within the presented errors. Based on these results we used the measured cross sections for $dd \to {}^3\mathrm{H}p$ to calculate the cross sections for $dd \to {}^3\mathrm{He}n$ at 1.2 GeV/c. For this the angular distributions for the beam momenta of 1.109 GeV/c, 1.387 GeV/c and 1.493 GeV/c were parametrized. Then, for selected polar angles the dependence of the differential cross section on the beam momentum was fitted and interpolated to the beam momentum of 1.2 GeV/c. The resulting distribution was used as an input for the simulation of $dd \to {}^3\mathrm{He}n$. Figure 2 (right) shows the match of the angular distribution of ^{3}He in data and the Monte-Carlo filtered event generator. The extracted integrated luminosity is determined to be $L^1_{int} = (877 \pm 2_{stat.} \pm 62_{sys.} \pm 62_{norm.})\ nb^{-1}$, where the superscript 1 refers to the first part of the run, see below. The systematic uncertainty reflects different parametrizations of the reference cross sections. In addition, the uncertainty of 7% in the absolute normalization of the reference data is also included. The result for the total cross section given below is based only on this first part of the run. The second part was optimized for high luminosities and also served as a pilot run for a measurement of $dd \to {}^4\mathrm{He}\pi^0$. It provided data to extract high statistics differential distributions for $dd \to {}^3\mathrm{He}n\pi^0$. These have been absolutely normalized relative to the first part of the run using the rates of the $dd \to {}^3\mathrm{He}n\pi^0$ reaction. The integrated luminosity obtained for the second part of the run amounts to $L^2_{int} = (4909 \pm 13_{stat.} \pm 350_{sys.} \pm 350_{norm.})\ nb^{-1}$.

The uncertainty on the integrated luminosity (in total 10% if all contributions are added quadratically) is the dominant source for the systematic error on the absolute normalisation. Another major source is associated with the cut on the cumulated probability distribution of the kinematic fit. In order to quantify the influence of this cut, the analysis was repeated for different regions in the probability distribution. For the total cross section the maximum deviation from the average value was taken as error. Changes in the shape of the differential distributions were extracted similarly, however excluding the variation in the absolute scale. For all other analysis conditions according to the criteria discussed in Ref. [18] no significant systematic effect was observed.

PHENOMENOLOGICAL MODELS

Presently, no theoretical calculation exists for a microscopic description of the investigated reaction. However, in order to have a sufficiently precise acceptance correction a model which reproduces the experimental data reasonably well is required. The ansatz used here is the incoherent sum of a quasi-free reaction mechanism based on $dp \to {}^3\mathrm{He}\pi^0$ and a partial-wave expansion for the 3-body reaction. While the latter is limited to s- and p-waves, the large relative momentum between the spectator nucleon and the rest system in the quasi-free model corresponds to higher partial waves motivating the incoherent sum and the neglection of interference terms.

Quasi-free reaction model

High momentum transfer reactions involving a deuteron can proceed via interaction with a single nucleon of the deuteron with the second nucleon being regarded as a spectator. Naturally, this mechanism is most significant in regions of the phase space where the momentum of one nucleon in final state matches the typical Fermi momenta in the deuteron. In the present experiment two deuterons are involved and, thus, the reaction may proceed with a projectile or target neutron spectator. For the parametrization of the quasi-free sub reaction $dp \to {}^3\mathrm{He}\pi^0$, the empirical angular distributions and the energy dependent cross section in the energy regime from threshold up to an excess energy of 10 MeV [20] and for excess energies of 40, 60 and 80 MeV [21] have been used. They have been convoluted with the momentum distribution of the proton in the deuteron using an analytical form of the deuteron wave function based on the Paris potential [19]. As a result one gets absolutely normalized differential cross sections for the quasi-free contribution to $dd \to {}^3\mathrm{He}n\pi^0$, which can be directly compared to the measured data. Figure 3 (left) shows the momentum distribution of the neutron for data and the quasi-free model filtered by Monte-Carlo. As expected the quasi-free process dominates the distribution for small momenta. The lower boundary of the spectrum

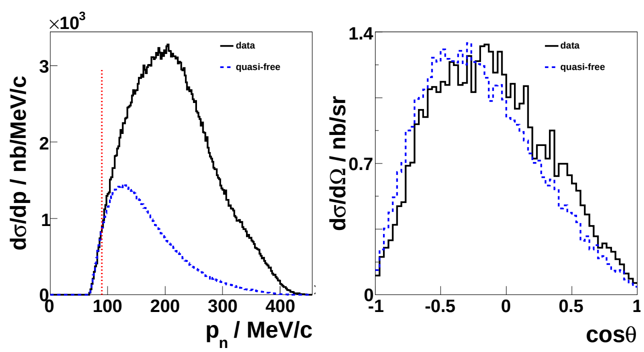

FIG. 3. Comparison of data (black line) and the quasi-free model filtered by Monte-Carlo (blue dashed line). Left: Momentum distribution of the neutron. Right: Angular distribution of the pion in the ${}^3\mathrm{He} - \pi^0$ subsystem for neutron momenta smaller than 90 MeV/c (indicated by the vertical red dashed line in the left plot). Data are not corrected for the acceptance.

is caused by kinematic effects. At a beam momentum of 1.2 GeV/c the reaction $dp \to {}^3\mathrm{He}\pi^0$ with the target proton at rest is below threshold and can only occur for $p_{\mathrm{fermi}} > 48$ MeV/c. The vanishing acceptance at $\theta_{^3\mathrm{He}} < 3^\circ$ further increases the minimum Fermi momentum. The right panel of Fig. 3 shows the angular distribution of the pion in the ${}^3\mathrm{He} - \pi^0$ subsystem for neutron momenta below 90 MeV/c, *i.e.* in the region where the quasi-free process should dominate the distribution.

Partial wave decomposition

For the remaining part of the data which cannot be described with a quasi-free process a 3-body model based on a partial wave decomposition has been developed. The relative angular momenta were defined according to the coordinates introduced earlier: one in the global π^0 - (${}^3\mathrm{He}n$) system and one in the ${}^3\mathrm{He}n$ subsystem (denoted by l and L, respectively). For the partial wave decomposition the angular momenta have been limited to $l + L \leq 1$, *i.e.* to at most one p-wave in the system. For the momentum dependence the standard approximation $|M|^2 \propto q^{2l} p^{2L}$ was used. Taking into account all possible spin configurations this results in 18 possible amplitudes. After combining the amplitudes with the same signature in final state, four possible contributions can be identified: s-wave in both systems (sS), one p-wave in either system (sP and pS) and a $sP - pS$ interference term. They can be described by seven real coefficients (four complex amplitudes minus one overall phase). With this the four-fold differential cross section can be written as:

$$\frac{d^4\sigma}{2\pi \; dM_{^3\mathrm{He}n} \; d\cos\theta_p \; d\cos\theta_q \; d\varphi} = C\,pq \Big[A_0 + A_1 q^2 + A_3 p^2 + \frac{1}{4} A_2 q^2 \left(1 + 3\cos 2\theta_q\right) + \frac{1}{4} A_4 p^2 \left(1 + 3\cos 2\theta_p\right) + A_5 pq \cos\theta_p \cos\theta_q + A_6 pq \sin\theta_p \sin\theta_q \cos\varphi \Big] \quad (1)$$

with

$$C = \frac{1}{32(2\pi)^5 s p_a^* (2s_a + 1)(2s_b + 1)} \quad (2)$$

where s_a and s_b denote the spin of beam and target and s and p_a^* the total energy squared and the beam momentum, respectively, in the c.m. system. The coefficients A_i describe the strength of the individual contributions mentioned above: A_0 corresponds to $l = L = 0$ (sS), A_1 and A_2 to $l = 1$ and $L = 0$ (pS), A_3 and A_4 to $l = 0$ and $L = 1$ (sP) and A_5 and A_6 to the interference term. Integration of Eq. 1 results in a set of equations for the description of the single differential cross sections:

$$\frac{d\sigma}{dM_{^3\mathrm{He}n}} = 16\pi^2 C pq \left[A_0 + A_1 q^2 + A_3 p^2\right] \quad (3a)$$

$$\frac{d\sigma}{2\pi d\cos\theta_q} = 4\pi C \left[B + \frac{1}{4} A_2 \left(1 + 3\cos 2\theta_q\right) I_{pS}\right] \quad (3b)$$

$$\frac{d\sigma}{2\pi d\cos\theta_p} = 4\pi C \left[B + \frac{1}{4} A_4 \left(1 + 3\cos 2\theta_p\right) I_{sP}\right] \quad (3c)$$

$$\frac{d\sigma}{d\varphi} = 8\pi C \left[B + \frac{\pi^2}{16} A_6 I_{pS+sP} \cos\varphi\right] \quad (3d)$$

with the new coefficient

$$B = A_0 I_{sS} + A_1 I_{pS} + A_3 I_{sP}. \quad (4)$$

The constants I_{sS}, I_{pS}, I_{sP} and I_{pS+sP} are the results of integration over $M_{^3\mathrm{He}n}$:

$$I_{sS} = \int_{(M_{^3\mathrm{He}} + M_n)^2}^{(\sqrt{s} - M_\pi)^2} pq \, dM_{^3\mathrm{He}n} \quad (5a)$$

$$I_{pS} = \int_{(M_{^3\mathrm{He}} + M_n)^2}^{(\sqrt{s} - M_\pi)^2} pq^3 \, dM_{^3\mathrm{He}n} \quad (5b)$$

$$I_{sP} = \int_{(M_{^3\mathrm{He}} + M_n)^2}^{(\sqrt{s} - M_\pi)^2} p^3 q \, dM_{^3\mathrm{He}n} \quad (5c)$$

$$I_{pS+sP} = \int_{(M_{^3\mathrm{He}} + M_n)^2}^{(\sqrt{s} - M_\pi)^2} p^2 q^2 \, dM_{^3\mathrm{He}n} \quad (5d)$$

Equations 3 do not contain the coefficient A_5 as the corresponding term vanishes with the integration over $cos\theta_q$ and $cos\theta_p$. In order to extract this coefficient Eq. 1 has to be multiplied by $cos\theta_q cos\theta_p$ before integration. This results in the following formula to determine A_5:

$$\frac{d\sigma'}{d\varphi} = \frac{8}{9}\pi C A_5 I_{pS+sP} \quad (6)$$

with $\sigma'(q,p) = \sigma(q,p) \cdot cos\theta_q cos\theta_p$.

It has to be noted that the coefficients A_0, A_1 and A_3 cannot be extracted unambiguously from the differential distribution $d\sigma/dM_{^3\mathrm{He}n}$. In the non-relativistic limit q^2 and p^2 are both linear in $M_{^3\mathrm{He}n}$ introducing a correlation of all three coefficients. For the measurement of $dd \to {}^3\mathrm{He}n\pi^0$ at an excess energy of $Q \approx 40$ MeV this is still a good approximation. Thus, only a value for B can be

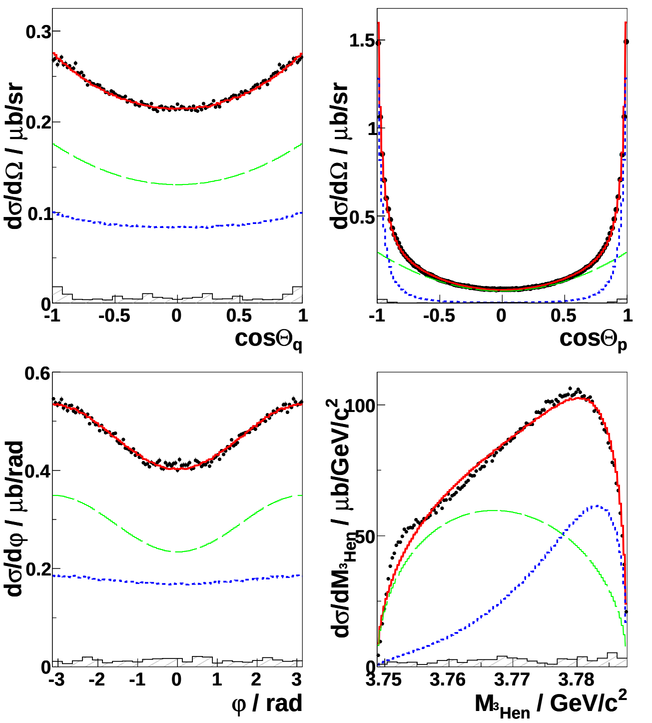

FIG. 4. Acceptance corrected data (black points) presented as functions of $M_{^3\mathrm{Hen}}$, $cos\theta_q$, $cos\theta_p$ and φ, respectively. The curves represent the fit to the model: full model (red solid), quasi-free contribution (blue dashed) and the partial wave decomposition (green long dashed). The hatched areas indicate the systematic uncertainties of the shape of differential distributions. Uncertainties on the absolute normalization are not included.

extracted from the data. Any values for A_0, A_1 and A_3 fulfilling Eq. 4 and the fit to $d\sigma/dM_{^3\mathrm{Hen}}$ will lead to the same model description.

RESULTS

In a first step a sum of Monte-Carlo filtered distributions for each contribution from the partial wave decomposition (coefficients A_0 to A_6) and from the quasi-free model (coefficient A_7) was fitted to the uncorrected, single differential spectra. The result served as input for the Monte-Carlo simulation finally used to determine the acceptance correction.

The final distributions after acceptance correction are presented in Fig. 4. Contributions from the quasi-free model, the partial wave decomposition and the full model are shown in blue, green and red, respectively. These spectra were refitted using the analytical formulas given in the previous section. The result is consistent with the previous fit. Although the partial wave expansion was limited to at most one p-wave in the final state it provides a reasonable overall description of the data: both angular distributions show a significant contribution of p-waves of similar size, the pS-sP interference term is visualized by the non-isotropic distribution of $d\sigma/d\varphi$. The quasi-free contribution is about 1.11 μb and, thus, is in agreement within the normalisation error of about 10% given in Ref. [20] with the prediction of the quasi-free model of 1.192 μb. The result of the fit using Eq. 6 and the quasi-free model to the data is presented in Fig. 5. The values for extracted coefficients from the global fit are summarized in Table I.

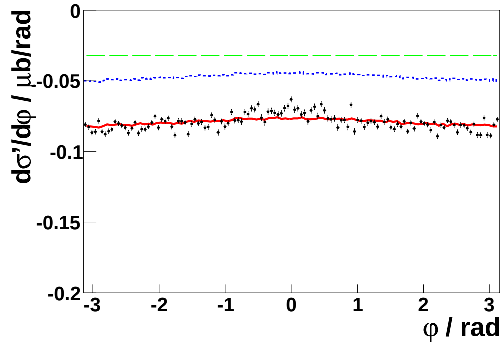

FIG. 5. Distribution of $d\sigma'/d\varphi$ as used in Eq. 6 to extract A_5.

One should emphasize that the meaning of the fit parameters is limited to the context of the discussed model. Any addition of higher partial waves, for example, would also change the extracted amplitudes of the lower partial waves. Thus, systematic errors are only provided for data. For the extracted fit parameters only statistical errors are given.

Contribution	**Fit results**	
sS,pS,Sp wave	$\mathbf{B}$ [μb] 1.840 ± 0.003	
sS wave	$\mathbf{A_0}$ [$\mu b/\mathbf{GeV^3}$] (0.41 ± 0.08)×10^4	
pS wave	$\mathbf{A_1}$ [$\mu b/\mathbf{GeV^5}$] (8.2 ± 7.0)×10^4	$\mathbf{A_2}$ [$\mu b/\mathbf{GeV^5}$] (18.3 ± 0.3)×10^4
sP wave	$\mathbf{A_3}$ [$\mu b/\mathbf{GeV^5}$] (1.08 ± 0.02)×10^4	$\mathbf{A_4}$ [$\mu b/\mathbf{GeV^5}$] (18.04 ± 0.07)×10^4
$pS + Sp$ interference	$\mathbf{A_5}$ [$\mu b/\mathbf{GeV^5}$] (-45.4 ± 0.3)×10^4	$\mathbf{A_6}$ [$\mu b/\mathbf{GeV^5}$] (-15.0 ± 0.2)×10^4
quasi free	$\sigma_{\mathbf{qf}} \cdot \mathbf{A_7}$ [μb] 1.108 ± 0.003	

TABLE I. Collection of the extracted fit parameters. The amplitudes are given in units of $(4\pi)^2C$. The parameters A_0, A_1 and A_3 are correlated and could not be extracted unambiguously, the given numbers represent one possible solution (see text).

So far, a possible momentum dependence of the transition amplitudes, for example due to initial or final state

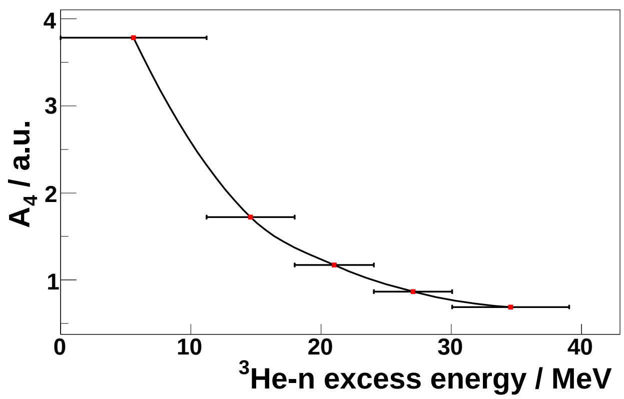

FIG. 6. Coefficient A_4 representing the p-wave contribution in the $^3\mathrm{He}-n$ system as a function of the excess energy. The error bars along the x-axis represent the width of the intervals in $M_{^3\mathrm{He}n}$.

interaction, was neglected. Deviations from this assumption were studied by refitting the data for five intervals in $M_{^3\mathrm{He}n}$ (corresponding to intervals in $\vec{q}$ and $\vec{p}$). All coefficients except one remained constant. Only A_4 representing a p-wave contribution in the $^3\mathrm{He}n$ system showed a significant momentum dependence (see Fig. 6): A_4 is larger for low excess energies in the $^3\mathrm{He}n$ system (corresponding to low relative momenta). One possible reason for this might be excited states with isospin $I = 1$ in the $^3\mathrm{He}n$ system at low excess energies as reported in Ref. [22] (the production of an $I = 0$ state would be charge symmetry breaking).

Integrating over the differential distributions we obtain for the total cross section of the $dd \to {}^3\mathrm{He}n\pi^0$ reaction:

$$\sigma_{tot} = (2.89 \pm 0.01_{stat.} \pm 0.06_{sys.} \pm 0.29_{norm})\ \mu b. \quad (7)$$

SUMMARY

For the first time an exclusive measurement of the $dd \to {}^3\mathrm{He}n\pi^0$ reaction has been performed. A total cross section of $\sigma_{tot} = 2.89\ \mu b$ with an accuracy of about 11% has been extracted. Differential distributions have been compared to the incoherent sum of a quasi-free reaction model and a partial-wave expansion limited to at most one p-wave in the final state. The contribution of the quasi-free processes accounts for about 1.11 μb of the total cross section matching the prediction of the quasi-free reaction model. The partial wave decomposition reveals the importance of p-wave contributions in the final state. The applied model shows a reasonable agreement for all differential distribution. Thus, based on this comparison no indication for significant contributions of higher partial waves can be deduced.

The whole data set amounts to about 3.4×10^6 fully reconstructed and background-free events. The presented differential distributions are only one possible representation of the results. One goal of the measurement was to provide data for studying dd initial state interaction for small angular momenta, which is one missing information in the microscopic description of the charge symmetry breaking reaction $dd \to {}^4\mathrm{He}\pi^0$ within the framework of Chiral Perturbation Theory. Once the important observables have been identified the corresponding experimental distributions can be provided.

ACKNOWLEDGEMENTS

We would like to thank the technical and administrative staff at the Forschungszentrum Jülich, especially at the COoler SYnchrotron COSY and at the participating institutes. This work has been supported in part by the German Federal Ministry of Education and Research (BMBF), the Polish Ministry of Science and Higher Education, Forschungszentrum Jülich (COSY-FFE) and the European Union Seventh Framework Programme (FP7/2007-2013) under grant agreement No. 283286.

* Electronic address: v.hejny@fz-juelich.de
† Present address: Department of Physics and Astrophysics, University of Delhi, Delhi–110007, India
‡ Present address: Department of Physics, Stockholm University, Roslagstullsbacken 21, AlbaNova, 10691 Stockholm, Sweden
§ Present address: Institut für Kernphysik, Johannes Gutenberg–Universität Mainz, Johann–Joachim–Becher Weg 45, 55128 Mainz, Germany
¶ Present address: Department of Physics and Astronomy, University of California, Los Angeles, California–90045, U.S.A.
** Present address: Albert Einstein Center for Fundamental Physics, Fachbereich Physik und Astronomie, Universität Bern, Sidlerstr. 5, 3012 Bern, Switzerland

[1] S. Weinberg, Trans. N.Y. Acad. Sci. **38** (1977) 185.
[2] J. Gasser and H. Leutwyler, Phys. Rep. **87** (1982) 77.
[3] H. Leutwyler, Phys. Lett. **B 378** (1996) 313.
[4] G. Miller et al., Phys. Rep. **194** (1990) 1.
[5] N. Fettes, U.-G. Meißner and S. Steininger, Phys. Lett. **B 451** (1999) 233; M. Hoferichter, B. Kubis and U.-G. Meißner, Phys. Lett. **B 678** (2009) 65.
[6] E. Stephenson etal., Phys. Rev. Lett. **91** (2003) 142302.
[7] A. Opper et al., Phys. Rev. Lett. **91** (2003) 212302.
[8] G.A. Miller et al., Ann. Rev. Nucl. Part. Sci. **56** (2006) 253.
[9] A. Filin et al., Phys. Lett. **B 681** (2009) 423.
[10] C. Hanhart et al., Phys. Rep. **397** (2004) 155.
[11] A. Gårdestig et al., Phys. Rev. **C 69** (2004) 044606.
[12] A. Nogga et al., Phys. Lett. **B 639** (2006) 465.
[13] T. A. Lahde and G. A. Miller, Phys. Rev. **C 75** (2007) 055204 [Erratum-ibid. **C 77** (2008) 019904].

[14] A. C. Fonseca, R. Machleidt and G. A. Miller, Phys. Rev. **C 80** (2009) 027001.
[15] R. Maier et al., Nucl. Phys. **A 626** (1997) 395c.
[16] H. H. Adam et al., arXiv: nucl-ex/0411038.
[17] G. Bizard et al., Phys. Rev.**C 22** (1980) 1632.
[18] R. Barlow, *Systematic errors: Facts and fictions* (2002), arXiv: hep-ex/0207026.
[19] M. Lacombe et al., Phys. Lett. **B 101** (1981) 139.
[20] V.N. Nikulin et al., Phys. Rev. **C 54** (1996) 1732.
[21] M. Betigeri et al., Nucl. Phys. **A 690** (2001) 473.
[22] D. R. Tilley et al., Nucl. Phys. **A 541** (1992) 1.